Self-similar temporal turbulent boundary layer flow

Damien Biau

Dynfluid Laboratory, École Nationale Superieure d'Arts et Métiers., 151 Boulevard de l'Hôpital, 75013 Paris, France

Boundary layers
Turbulent boundary layers
Self-similar solution

Direct numerical simulations of temporally evolving boundary layer flows are considered with solutions restricted to self-similar profiles. A new set of modified Navier–Stokes equations is solved with periodic boundary conditions in the streamwise direction, and solutions reach statistically steady states, independent of the initial conditions. The results are presented for different cases, with and without a pressure gradient, and found to be in agreement with existing results of spatial turbulent boundary layer flows. Thus, self-similar temporal solutions are able to reproduce the general features of turbulent boundary layer flows. Finally, the model is applied to simulate a turbulent spot in equilibrium, which is difficult to obtain otherwise.

1. Introduction

In his famous memoir on the effect of air on the motion of pendulums, Stokes [1] also introduced in a note the resolution of the incompressible temporal boundary layer over an impulsively started flat plate. That analytical solution is currently known as the error function, so named by Glaisher [2]. Later, Rayleigh [3] applied the results by Stokes to a case where a force propelling a plane is given, taking as an example the sudden fall of lamina under the action of gravity. Blasius [4,5], following the work of his supervisor Ludwig Prandtl on boundary layer equations, showed an easier method of solution using similarity transformation. The original system of partial differential equations was then reduced to an ordinary second-order differential equation, and this method is currently found in many textbooks; see, for example, the monography by Schlichting [6].

The Stokes solution is valid if the plate is infinite in extent and does not take the leading-edge effect into account. In the case of a semi-infinite flat plate, the development of a flow from the initial Stokes solution to the ultimate Blasius solution was analytically investigated by Stewartson [7,8]. The results agreed with the numerical resolution by Dennis [9] for unsteady boundary layer equations. The calculations of Dennis [9] have shown a quick transition to the steady spatial solution; thus, the transient is marginally relevant in a general study of boundary layer flows. Nonetheless, despite its limited scope of applications, the temporal boundary layer is still a regular subject of investigations, mainly motivated by the simplification of the streamwise homogeneity.

The linear stability analysis of the unsteady Stokes solution has been investigated by Otto [10] with a quasi-steady approach, and the perturbations are a solution of the classic Orr–Sommerfeld equation linearized around a frozen laminar solution. The method was improved by Luchini and Bottaro [11] with a multiple-scale approach to consider the temporal growth of the boundary layer. That correction shows slight modification of the critical Reynolds number, which was found to be lowered by 2%.

Beyond the linear analysis, numerical simulations of the full Navier–Stokes equations have been performed. In fact, preliminary simulations of transitions in boundary layer flow have used the temporal approach; see the review by Kleiser and Zang [12]. The numerical results have shown good agreement with experimental measurements and flow visualizations at corresponding stages of development. Thus, despite their limitations, these studies have achieved some notable successes, advancing to the accurate simulation of the complete transition to turbulence.

Kozul et al. [13] performed the first direct numerical simulations (DNS) of the incompressible temporally developing turbulent boundary layer as a counterpart to the spatially developing boundary layer in a similar spirit to those temporal counterparts studied for canonical free-shear flows, see [14,15] among others. The transport of a passive scalar is also simulated. The initial laminar flow is perturbed with a wall-mounted trip which triggers transition to turbulence and after an initial transient, a developed turbulent state settles. Kozul et al. [13] compared the results with those obtained in spatial framework by Schlatter and Örlü [16] at two Reynolds numbers, $Re_\theta = 1000$ and 2000, based on the momentum thickness and the free-stream velocity. Comparisons of the skin friction coefficient, velocity and scalar statistics demonstrate that the temporally developing boundary layer is a good model for the spatially developing boundary layer. Kozul et al. [13] suggest that the spatial and temporal boundary layer becomes similar at high Reynolds numbers, when the ratio between the skin

E-mail address: damien.biau@ensam.eu.

friction velocity and the free stream velocity tends to zero. Nonetheless, the advantage of the temporal DNS comes with some issues. The final boundary layer thickness for a desired final Reynolds number is not known a priori. Additionally, the grid must be calibrated for that final boundary layer thickness and final Reynolds number; thus, the domain size and the resolution are oversized during the initial transient before the developed turbulence. Moreover, the influence of the initial forcing necessary to trigger the transition remains for a long time, but the flow eventually reaches a fully developed Couette flow. These two constraints result in a limited temporal range to obtain statistically converged results.

Topalian et al. [17] solved this difficulty considering a temporal slow-growth formulation of the compressible Navier–Stokes equations, thus adapting the seminal work by Spalart [18] dedicated to the incompressible spatial boundary layer flow. The shift to a temporal framework avoids a complication inherent in the spatial case since the additional temporal slow-growth terms leave the mass continuity equation unchanged, which facilitates implementation in an existing solver. Indeed, the equations obtained by Topalian et al. [17] only introduce an additional parameter, the temporal growth of the boundary layer thickness. That method has been applied to two problems: an essentially incompressible, zero-pressure-gradient boundary layer (at $Re_\theta = 422$ and 703) and a transonic boundary layer over a cooled, transpiring wall. The results show that the approach produces flows that are qualitatively similar to other slow-growth methods as well as spatially developing simulations. The temporal slow-growth model flow is able to reproduce many of the important features of the statistics of a zero-pressure-gradient, spatially evolving boundary layer. Topalian et al. [17] shown that the mean velocity, the streamwise rms velocity, and dominant near-wall terms in the kinetic energy budget are well-represented. They also shown that the Reynolds shear stress, wall-normal rms velocity, and spanwise rms velocity are lower in the temporal simulation than in the spatially homogenized or spatially evolving cases. The temporal slow-growth model by Topalian et al. [17] is an important improvement for studying wall-bounded turbulence more generally or for RANS model evaluation. Nonetheless, Topalian et al. [17] did not relate the thickness growth to the characteristic length of the flow, so the relation with nondimensionalization, such as the Reynolds number, is not obvious. As a consequence, the equations introduced by Topalian et al. [17] are governed by two non-dimensional parameters, the Reynolds number and the non-dimensional thickness growth, the latter being not a control parameter of the flow. The lack of an explicitly defined boundary layer thickness introduces a difficulty when considering the extension of the method to more general boundary layer with pressure gradient because the non dimensionalization of the external pressure gradient is not obvious. Moreover, Topalian et al. [17] restricted the self-similar assumption to the averaged velocity profiles which does not permit an extension to transient flows such as the transition to turbulence or flows with unsteady boundary conditions.

In the present work, the instantaneous wall-normal profiles are assumed to be self-similar. Similarity analyses of turbulent shear flows can be found in [19,20]. The momentum thickness θ is used as the reference length scale; as a consequence, the nondimensional temporal thickness growth is calculated so that the nondimensional momentum thickness remains unitary. Hence, the model presented in the next section is free from arbitrariness, consistent with nondimensionalization and adapted to the transient behaviors encountered, such as in the laminar–turbulent transition or with unsteady boundary conditions.

Before introducing the equations in the next section, it is worth mentioning the main limitation of the self-similarity applied to wall bounded flows. While self-similarity is exact for the laminar solution, as shown by Blasius, it is highly questionable in turbulent regimes. The loss of momentum at the wall results in an additional characteristic length-scale for the inner layer, based on the wall shear stress and the kinematic viscosity. Two distinct length scales make exact self-preservation impossible; however, the self-similar transformation acts mainly in the outer layer, where it is physically relevant. For the purposes of validation, the results are compared with existing results of spatial turbulent boundary layer flows in the third section.

2. Method

We consider a wall impulsively stopped beneath a fluid moving at constant velocity. The wall is assumed to be infinite, so the leading-edge effect is neglected. Because of the no-slip boundary condition, a temporal boundary layer develops, characterized by the kinematic viscosity ν. The characteristic velocity is U_∞, the asymptotic streamwise velocity far from the wall. The length scale is defined as the momentum thickness; note that displacement thickness can be used as well.

The usual nondimensional set of Cartesian coordinates (x, y, z) and nondimensional velocity components $\mathbf{u} = (u, v, w)$ are adopted in the streamwise, wall-normal and spanwise directions.

The temporal boundary layer simulations realized in the finite domain in the wall normal direction eventually evolve towards a linear velocity profile. To obtain statistically steady boundary layer solutions, the velocity field is assumed to be instantaneously adapted to the boundary layer growth, so the solution exhibits a self-similar profile in the wall normal direction:

$$\mathbf{u}(x, y, z, t) \to \mathbf{u}\left(x, \frac{y}{\theta(t)}, z, t\right) \tag{1}$$

To be consistent with the nondimensionalization, θ corresponds to the nondimensional momentum thickness,

$$\theta = \int_0^\infty U\,(1 - U)\,dy \tag{2}$$

$U = < u >$ is the streamwise and spanwise averaged nondimensional streamwise velocity.

The time derivative of the self-similar velocity (1) results a in fast time term and a slow-growth term decomposition:

$$\frac{\partial \mathbf{u}}{\partial t} \to \frac{\partial \mathbf{u}}{\partial t} - \dot{\theta}\ \frac{y}{\theta^2}\ \frac{\partial \mathbf{u}}{\partial (y/\theta)}$$

That slow-growth formulation is based on the assumption that the boundary layer grows much more slowly than the evolution of the turbulence; see also Topalian et al. [17]. The time derivative in the momentum equations introduces the nondimensional thickness growth $\dot{\theta}$, which is computed so that the self-similar renormalization $\theta = 1$ is fulfilled at each time.

The nondimensional Navier–Stokes equations, restricted to self-similar solutions in the wall-normal direction, take the form

$$\begin{aligned} &\nabla \cdot \mathbf{u} = 0 \\ &\frac{\partial \mathbf{u}}{\partial t} - \dot{\theta}\ y\ \frac{\partial \mathbf{u}}{\partial y} + \mathbf{u} \cdot \nabla \mathbf{u} = -\nabla p + Re^{-1} \nabla^2 \mathbf{u} \end{aligned} \tag{3}$$

The self-similar transformation appears in the equations only with the slow-growth term $-\dot{\theta}\ y\ \partial \mathbf{u}/\partial y$, which acts as an advection force towards the wall, balancing diffusion. We could have used dedicated notation for the self-similar coordinate $y/\theta(t)$, but since the nondimensional momentum thickness θ is maintained as unitary, we keep the notation y for simplicity. These Navier–Stokes equations are associated with impermeable and no-slip boundary conditions on the wall $\mathbf{u}(y = 0) = [0, 0, 0]$ and the far-field condition $\mathbf{u}(y \to \infty) = [1, 0, 0]$. The far-field boundary conditions are simpler here compared to the spatial case, which requires suction at the top boundary to avoid spurious acceleration induced by the downstream thickness growth.

The Navier–Stokes equations (3), with boundary and initial conditions is complete but $\dot{\theta}$ is implicitly known through the condition $\theta = 1$. Thus, $\dot{\theta}$ can be calculated with a bisection method, however, performing such iterative method directly on the Navier–Stokes equations would be numerically prohibitive, instead it is much more convenient to use the streamwise and spanwise averaged equation. The equation

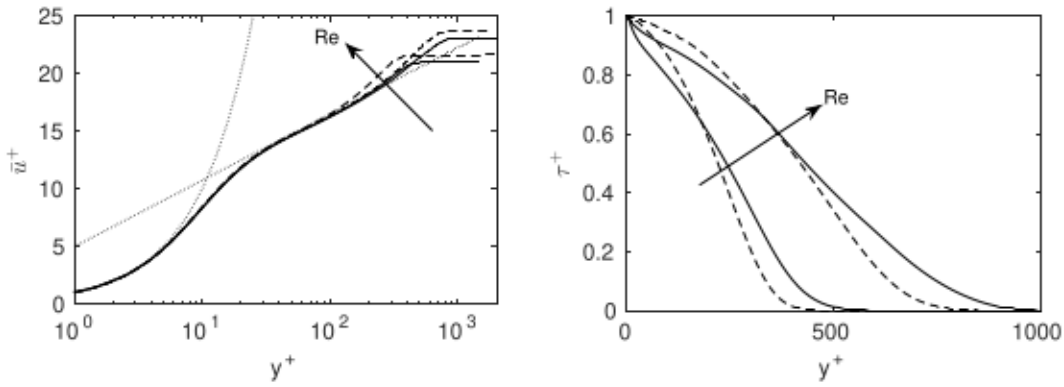

Fig. 1. Boundary layer with zero pressure gradient. Inner-scaled mean streamwise velocity ($\overline{u}^+$) and total shear stress ($\overline{\tau}^+$) at Reynolds numbers 1000 and 2000. Continuous lines, present results, dashed lines results by Schlatter and Örlü [16].

for the mean flow $U =< u >$, *i.e.*, the streamwise and spanwise averaged streamwise velocity, is

$$\frac{\partial U}{\partial t} - \dot{\theta}\ y\ \frac{\partial U}{\partial y} + \frac{\partial < uv >}{\partial y} = \frac{1}{Re}\frac{\partial^2 U}{\partial y^2} \tag{4}$$

The associated nondimensional boundary conditions are $U(y = 0) = 0$ and $U(y \to \infty) = 1$. All terms in the averaged Eq. (4) are known excepted $\dot{\theta}$ and U at the next time step. The mean velocity U at the previous time steps and the Reynolds stress $< uv >$ come from the Eqs. (3) and there is no need for a turbulence model. A bisection method is applied to compute $\dot{\theta}$, and the iterations are stopped when $|\theta - 1| \leq 10^{-14}$. Thus, the averaged Eq. (4), associated with bisection method to compute $\dot{\theta}$, is solved together with the Navier–Stokes equations (3). A less efficient but simpler alternative would be to solve $\dot{\theta}(t + \Delta t) = \dot{\theta}(t) + \alpha(\theta(t) - 1)$, with $\alpha \approx \Delta t$, that has been successfully tested but not used for the results shown hereafter.

Since the momentum thickness is not usual for the nondimensionalization of the Stokes problem, it may be useful to give the expression of the laminar solution of Eq. (4),

$$U_{lam} = \mathrm{erf}\left(\sqrt{\dot{\theta}_{lam}\ Re/2}\ y\right) \tag{5}$$

With $\dot{\theta}_{lam} = 0.1092267/Re$. That laminar profile is a self-similar solution of the first type since the thickness growth rate can be obtained from dimensional analysis, $\dot{\theta}_{lam} \propto Re^{-1}$. For turbulent regimes, The self-similar solution is of the second type [21], and the scaling law must be determined from numerical simulations.

The equations are solved with a Chebyshev collocation method in the wall-normal direction (y) and a Fourier pseudospectral method in the homogeneous streamwise (x) and spanwise (z) directions. The time-marching is a second-order finite difference scheme with a viscous term treated implicitly. Further details can be found in [22]. The numerical parameters are indicated, case by case, in the following section.

The initial velocity field consists in the laminar solution plus random fluctuations. Once the velocity field reaches the statistically steady state, the equations are integrated further in time to obtain a running time average of the various statistical correlations, which are independent of numerical initialization.

3. Results

For validation purposes, the model is applied to three problems whose results are of independent interest. First, turbulent simulations with zero pressure gradient are obtained for Reynolds numbers $Re_\theta = 1000$ and 2000, followed by a case with adverse pressure gradient at $Re_\theta = 1400$. Finally, a turbulent spot is obtained at $Re_\theta = 120$.

In the following, the overbar indicates streamwise, spanwise and temporal averaging. The relevant velocity and length scales close to the wall are obtained from the wall shear stress $\tau_w = \mu(d\bar{u}/dy)|_{y=0}$, leading to $u_\tau = \sqrt{\tau_w}/\rho$ and $l_\tau = \nu/u_\tau$. Quantities in wall scaling, referenced with the + superscript, are thus written as, e.g., $u^+ = u/u_\tau$ and $y^+ = y/l_\tau$.

Table 1
Some computed time-averaged parameters. Present temporal simulations/spatial simulations by Schlatter and Örlü [16]. The nondimensional thickness temporal growth $\dot{\theta}$, specific to the present simulations, is also indicated.

Re_θ	H	u_τ	τ_{rms}	$\dot{\theta}$
1000	1.4253/1.4499	0.0476/0.0462	0.4023/0.4059	1.5971
2000	1.3835/1.4135	0.0433/0.0421	0.4194/0.4146	1.3651

3.1. Boundary layer without pressure gradient

The domain size is $Lx = 70$, $Ly = 30$ and $Lz = 40$. The number of points in the x-, y-, and z-directions are $256 \times 150 \times 256$ for Reynolds number $Re_\theta = 1000$ and $512 \times 300 \times 512$ for $Re_\theta = 2000$, while the time steps are $\Delta t = 0.02$ and $\Delta t = 0.005$, respectively. The results are compared with the spatial direct simulations by Schlatter and Örlü [16] at identical Reynolds numbers. Other reference results were obtained by Simens et al. [23], similar to those obtained by Schlatter and Örlü [16]; thus, they will not be shown for clarity.

The mean streamwise velocity profiles, in wall units, are displayed in Fig. 1. The agreement with the reference results is correct in the buffer layer ($y^+ < 30$) and just above in the log layer. Farther from the wall, in the wake region, the self-similar solution scaled with the skin friction velocity is significantly below, which reflects the overestimation of the skin friction velocity. The difference with the spatial boundary layer is more pronounced for the total shear stress ($\tau = Re^{-1}d\bar{u}/dy - \overline{uv}$), displayed in the right part of Fig. 1. The averaged streamwise momentum gives the equation for the momentum flux,

$$\frac{d\tau}{dy} = -\dot{\theta}y\frac{d\bar{u}}{dy}. \tag{6}$$

The effect of the slow-growth term on the right-hand side acts mainly in the outer layer and linearly vanishes towards the wall, which explains the excessive negative slope that appears near the wall in the total stress profile. The same behavior was observed by Topalian et al. [17] and Kozul [24].

The mean and root-mean-squared (rms) velocity profiles are shown in Fig. 2 with inner scaling, which confirms the previous observations.

Some quantitative comparisons are also proposed in Table 1. The shape factor H, *i.e.* , the ratio between the displacement δ_1 and the momentum thicknesses θ, is an indicative parameter for the analysis of boundary layer flows. In the laminar regime, the shape factor takes the value 2.41 for the temporal boundary layer and 2.59 for the Blasius boundary layer. In the turbulent regime, values move closer, and the self-similar temporal boundary layer seems to approach the spatial case. The skin friction velocity, u_τ, is slightly overestimated compared to the value found by Schlatter and Örlü [16], as seen on the mean velocity profile, scaled in wall units, in Fig. 1. As an additional comparison, the

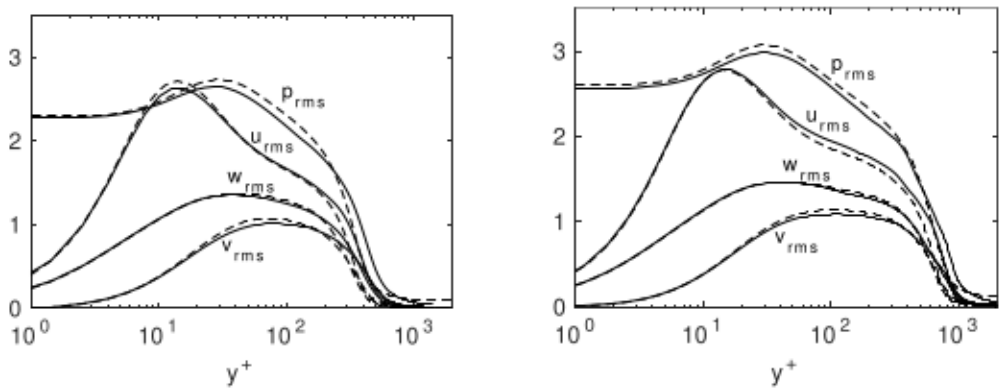

Fig. 2. Boundary layer with zero pressure gradient. Root-mean-squared velocity profiles at Reynolds numbers 1000 (left) and 2000 (right). Continuous lines, present results. Dashed lines result from Schlatter and Örlü [16].

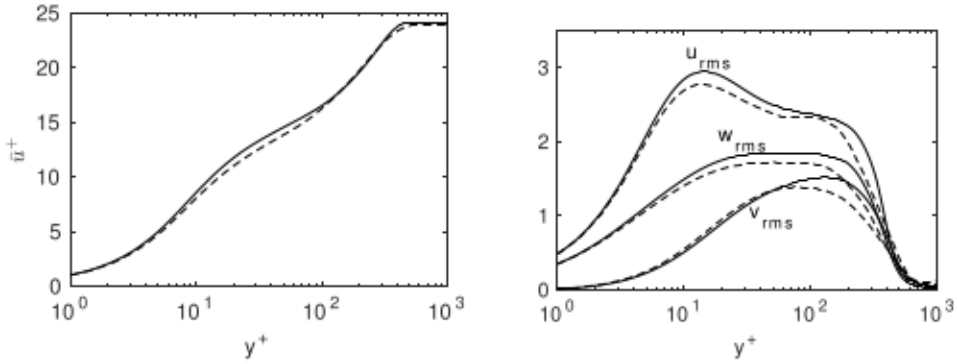

Fig. 3. Boundary layer with adverse pressure gradient. Inner-scaled mean streamwise velocity and root-mean-squared velocity profiles. Continuous lines, present results. Dashed lines result from Spalart and Watmuff [25].

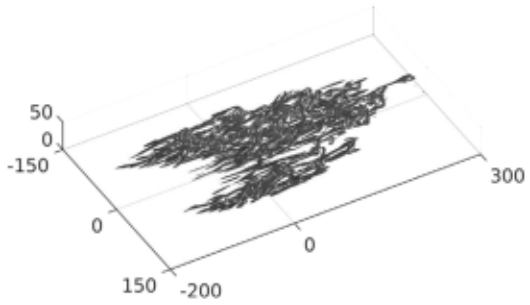

Fig. 4. Turbulent spot at $Re_\theta = 120$, where the fluid is moving from left to right. The vortical structures are visualized by the isosurface of the Q criterion.

normalized shear-stress fluctuation, defined by Alfredsson et al. [26] as $\tau^+_{w,rms} = \lim_{y\to 0} u_{rms}/U$, is found to be in good agreement, which confirms the realistic behavior of the self-similar turbulent boundary layer in the near-wall region. The nondimensional boundary layer growth rate, $\dot{\theta}$, decreases with increasing Reynolds number, as shown in Table 1. Hence, the influence of the slow growth term is gently reduced with large Reynolds numbers, so the exaggerated momentum flux at the wall normal is presumed to reduce in the limit of high Reynolds numbers.

3.2. Boundary layer with adverse pressure gradient

With a pressure gradient, the far-field velocity (noted U_0) is no longer constant in time; then, the equation for the self-similar base flow $U_0(t)\, U[t,\ y/\theta(t)]$, now takes the form:

$$\frac{\partial U}{\partial t} - \dot{\theta}\, y\, \frac{\partial U}{\partial y} + \dot{U}_0\, U + \frac{\partial < uv >}{\partial y} = -\frac{dP}{dx} + \frac{1}{Re}\frac{\partial^2 U}{\partial y^2}$$

The far-field limit gives $\dot{U}_0 = -dP/dx$. This results in an additional term on the right-hand-side of the streamwise momentum equation, keeping the same boundary conditions:

$$\frac{\partial U}{\partial t} - \dot{\theta}\, y\, \frac{\partial U}{\partial y} + \frac{\partial < uv >}{\partial y} = -\frac{dP}{dx}(1-U) + \frac{1}{Re}\frac{\partial^2 U}{\partial y^2} \tag{7}$$

The physical non dimensional parameters are $Re_\theta = 1400$ and $dP/dx = 2.2 \times 10^{-3}$ to match the value used by Spalart and Watmuff [25] at x=0.9, the pressure gradient has been normalized with the local free-stream velocity and momentum thickness. The domain size is $Lx = 100$, $Ly = 30$ and $Lz = 50$, and the number of points in the x-, y-, and z-directions are $512 \times 200 \times 512$ with a time step $\Delta t = 0.005$. The mean velocity profiles and rms fluctuations are shown in Fig. 3 and present good agreement with the spatial numerical results by Spalart and Watmuff [25], although the second peak on the streamwise fluctuations is absent from the self-similar solution. The shape factor is $H = 1.53$, compared to $H = 1.55$ [25], while the nondimensional pressure gradient is $\beta = \delta_1/\tau_w\, dP/dx = 1.94$ in our case and equal to 2 in [25].

3.3. Turbulent spot

To illustrate the possibility offered by the model, the simulation of a localized turbulence, or spot, with zero pressure gradient at a low Reynolds number is now presented. Turbulent spots were first observed by Emmons [27] in shallow water flowing down an inclined plate. That case moves away from the domain of validity of the model because of the low Reynolds number value; nonetheless, that compromise is

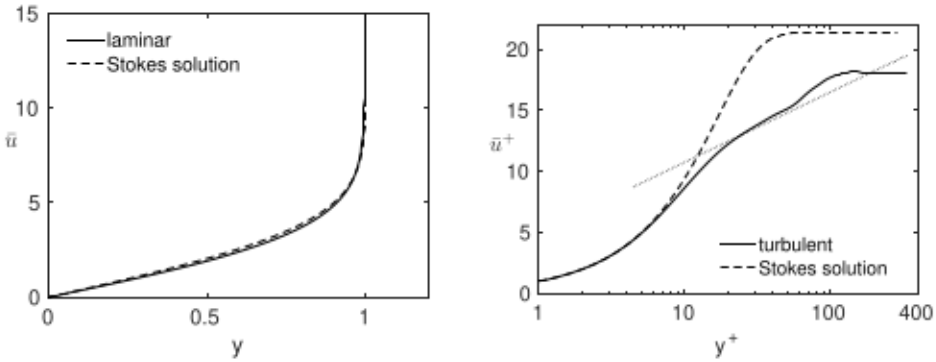

Fig. 5. Conditionally averaged streamwise velocity profiles for laminar (left) and turbulent (right) regions. The Stokes erf profile (see Eq. (5)) is also depicted for comparisons.

compensated for by the possibility of obtaining a converged turbulent spot, independent of the initial condition, which is impossible to obtain otherwise.

The domain size is larger than in the previous paragraphs with $Lx = 1200$, $Ly = 50$ and $Lz = 400$. The number of points in the x-, y-, and z-directions is $2048 \times 100 \times 1024$ with a time step $\Delta t = 0.01$. In the turbulent region, the maximal spacing between collocation points, in wall units, is $\Delta x^+ < 7$ and $\Delta z^+ < 4.6$; in the wall-normal direction, there are at least 20 non-uniformly spaced points within 12 wall units.

To reach a turbulent regime close to its onset, the Reynolds number is slowly decreased, starting from Re=300. For $Re_\theta < 160$, turbulence condenses in the spanwise direction, and for $Re_\theta < 130$, it also localizes in the streamwise direction. The minimal value for the sustained spot is $Re_\theta = 120$, and the turbulent patch is localized in both homogeneous directions. At such low Reynolds number the laminar flow is linearly stable, and the turbulent state is a relative attractor coexisting with the laminar basin of attraction, see Biau [28]. After a transient, the overall shape does not change in time, and the turbulent spot exhibits features independent of the initial condition, which appears as a universal structure in a laminar boundary layer. A snapshot of the three-dimensional vortical structures identified by the Q-criterion [29] is shown in Fig. 4.

In this figure, the flow direction is from the bottom left to the top right. The spot has a characteristic arrowhead shape, with the apex of the arrow oriented in the downstream direction, as for the zero-pressure-gradient boundary layer [30]. In addition to the overall shape of the spot, Fig. 4 also reveals streak-like structures elongated in the flow direction. In front of a spot, where the flow is still laminar, elongated streaks extending nearly to the size of the shear layer are observed. Further downstream towards the back side of the spot, where reverse transition from the turbulent to the laminar state occurs, turbulent fluctuations vanish, leading to the reappearance of streaky patterns, which are less sensitive to viscous damping. They are reminiscent of the streaks observed near the wall in turbulent boundary layers. The vortex structures present some Λ-vortices that are typically observed in transitional regimes. Close to the wall we have the typical low- and high-speed streaks turbulent spots feature generic small-scale coherent structures in the form of elongated counter-rotating vortices.

The normal velocity v has significant fluctuations only in the turbulent region, making it suitable as a marker of the interface between laminar and turbulent flow. The intermittency function is then defined as $I = 1$ where $E_v \geq 0.2 \max(E_v)$, elsewhere I=0; with $E_v = \int_y v^2 \, dy$. Conditionally averaged streamwise velocity profiles in both the laminar and turbulent area are shown in Fig. 5. Despite the low Reynolds number, the mean flow presents the characteristics of a developed turbulent wall flow, *i.e.* the linear region close to the wall and the (small) log region away from the wall, as observed by Wygnanski et al. [31].

In order to estimate the propagation velocity, the streamwise transport term in the Navier–Stokes equations (3) is modified: $u\partial_x \rightarrow (u-c)\partial_x$. The constant velocity c is adjusted in such that the spot is no more traveling. The propagation velocity is found as 70% of the free stream velocity, in agreement with the 65% value reported by Wygnanski et al. [31].

4. Conclusion

This article presents direct numerical simulations of a temporally evolving boundary layer restricted to self-similar solutions. In the turbulent regime, the solution evolves to a statistically steady state. That solution represents the intermediate-asymptotic behavior of the Navier–Stokes solution in the sense that the solution is no longer dependent on the details of the initial condition, but the system is not in the state of equilibrium reached at infinite Reynolds number; see Barenblatt and Zel'dovich [21].

The results are illustrated with simulations at moderate Reynolds numbers and compared to the spatial boundary layer, with and without a pressure gradient. Peculiar features of boundary layer flows are conserved, and the mean and fluctuation profiles are found to be in correct agreement with the spatial case. The log layer of the mean profile as well as the peaks in the fluctuation profiles are reproduced. The most notable difference is observed for the total shear stress, which presents a negative slope at the wall as a direct effect of the slow growth term added in the Navier–Stokes equations. As a consequence, the skin friction velocity is overestimated. Nonetheless, the amplitude of the slow-growth term decreases with increasing Reynolds numbers. Simulations at higher Reynolds number values could provide information on the asymptotic similarity of the turbulent boundary layers. In particular, the implications of competing inner and outer scales on profile invariance are still the subject of debate; see, for example, the discussions in [32,33].

By considering the numerical advantage of the present model, a streamwise-shortened domain is combined with periodic boundary conditions, and keeping in mind its limits, further applications can be considered. The slow-growth term can be added, in conjunction with the recycling method [23], to generate the inflow conditions for spatially developing simulations. Application to more complex flows could include system rotation, curvature, thermal stratification and unsteady boundary conditions. The numerical simplification can also be pushed forward in association with turbulent models. Since the self-similar assumption permits a local simulation of the boundary layer, the flow over an airfoil at a realistic Reynolds number could be performed at different streamwise locations with independent simulations.

Temporal simulation with the self-similar assumption is more reliable for free shear flow. All free shear layers, regardless of how they are generated, should asymptotically achieve the same self-preserving state; see many examples in the book by Townsend [19]. However, even if the self-preserving property of the flow is satisfied, the slow-growth condition assumption is not always observed. As an example, for the mixing layer, Rogers and Moser [14] found a value independent of the Reynolds number, $\hat{\theta} = 0.014$, which is too strong for the

turbulent fluctuations to adapt quickly to the thickness growth; thus, slow processes such as vortex merging are not compatible with the present model. The application to the far-wake seems more promising and could extend the work by Redford et al. [15] and Nedić et al. [34] on the existence of a universal asymptotic turbulent wake.

CRediT authorship contribution statement

Damien Biau: Conceptualization, Methodology, Writing.

Declaration of competing interest

The authors declare that they have no known competing financial interests or personal relationships that could have appeared to influence the work reported in this paper.

Data availability

Data will be made available on request.

Acknowledgments

The author is thankful to Professor Eric Lamballais for his persevering encouragement during the redaction of the present article.

References

[1] Stokes GG. On the effect of internal friction of fluids on the motion of pendulums. Trans Camb Phil Soc 1851;9:8–106.
[2] Glaisher JWL. On a class of definite integrals. Philos Mag J Sci 1871;42(280):294–302.
[3] Rayleigh JW Lord. On the motion of solid bodies through viscous liquid. Phil Mag 1911;21(126):697–711.
[4] Blasius H. Grenzschichten in Flüssigkeiten mit kleiner Reibung. Z Math Phys 1908;56:1–37.
[5] Blasius H. The boundary layer in fluids with little friction. Tech. rep., NACA; 1950.
[6] Schlichting H. Boundary–layer theory. 7th ed.. New York, USA: McGraw-Hill; 1979.
[7] Stewartson K. On the impulsive motion of a flat plate in a viscous fluid. Quart J Mech Appl Math 1951;4(2):182–98.
[8] Stewartson K. On the impulsive motion of a flat plate in a viscous fluid. II. Quart J Mech Appl Math 1973;26(2):143–52.
[9] Dennis SCR. The motion of a viscous fluid past an impulsively started semi-infinite flat plate. IMA J Appl Math 1972;10(1):105–17.
[10] Otto S. On the stability of a time dependent boundary layer. Tech. rep., ICASE; 1993.
[11] Luchini P, Bottaro A. Linear stability and receptivity analyses of the Stokes layer produced by an impulsively started plate. Phys Fluids 2001;13(6):1668–78.
[12] Kleiser L, Zang TA. Numerical simulation of transition in wall-bounded shear flows. Annu Rev Fluid Mech 1991;23(1):495–537.
[13] Kozul M, Chung D, Monty JP. Direct numerical simulation of the incompressible temporally developing turbulent boundary layer. J Fluid Mech 2016;796:437–72.
[14] Rogers Michael M, Moser Robert D. Direct simulation of a self-similar turbulent mixing layer. Phys Fluids 1994;6(2):903–23.
[15] Redford John A, Castro Ian P, Coleman Gary N. On the universality of turbulent axisymmetric wakes. J Fluid Mech 2012;710:419–52.
[16] Schlatter P, Örlü R. Assessment of direct numerical simulation data of turbulent boundary layers. J Fluid Mech 2010;659:116–26.
[17] Topalian V, Oliver Todd A, Ulerich Rhys, Moser Robert D. Temporal slow-growth formulation for direct numerical simulation of compressible wall-bounded flows. Phys Rev Fluids 2017;2:084602.
[18] Spalart PR. Direct numerical simulation of turbulent boundary layer up to Re_θ=1410. J Fluid Mech 1988;187:61–98.
[19] Townsend AA. The structure of turbulent shear flows. Cambridge University Press; 1956.
[20] George WK. The self-preservation of turbulent flows and its relation to initial conditions and coherent structures. Adv Turbulence 1989;39–72.
[21] Barenblatt GI, Zel'dovich YB. Self-similar solutions as intermediate asymptotics. Annu Rev Fluid Mech 1972;4(1):285–312.
[22] Biau D. Transient growth of perturbations in Stokes oscillatory flows. J Fluid Mech 2016;794:R4.
[23] Simens MP, Jiménez J, Hoyas S, Mizuno Y. A high-resolution code for turbulent boundary layers. J Comput Phys 2009;228:4218–31.
[24] Kozul M. The turbulent boundary layer studied using novel numerical frameworks (Ph.D. thesis), University of Melbourne; 2018.
[25] Spalart PR, Watmuff JH. Experimental and numerical study of a turbulent boundary layer with pressure gradients. J Fluid Mech 1993;249:337–71.
[26] Alfredsson P Henrik, Johansson Arne V, Haritonidis Joseph H, Eckelmann Helmut. The fluctuating wall-shear stress and the velocity field in the viscous sublayer. Phys Fluids 1988;31(5):1026–33.
[27] Emmons HW. The laminar-turbulent transition in a boundary layer-part I. J Aeronaut Sci 1951;18(7):490–8.
[28] Biau D. Laminar-turbulent separatrix in a boundary layer flow. Phys Fluids 2012;24(3):034107.
[29] Hunt JCR, Wray A, Moin P. Eddies, streams, and convergence zones in turbulent flows. Tech. rep. CTR-S88, Center for Turbulence Research; 1988.
[30] Elder JW. An experimental investigation of turbulent spots and breakdown to turbulence. J Fluid Mech 1960;9(2):235–46.
[31] Wygnanski I, Sokolov M, Friedman D. On a turbulent 'spot' in a laminar boundary layer. J Fluid Mech 1976;78(4):785–819.
[32] George WK, Castillo L. Zero-pressure-gradient turbulent boundary layer. ASME Appl Mech Rev 1997;50:689–729.
[33] Jones MB, Nickels TB, Marusic Ivan. On the asymptotic similarity of the zero-pressure-gradient turbulent boundary layer. J Fluid Mech 2008;616:195–203.
[34] Nedić J, Vassilicos JC, Ganapathisubramani B. Axisymmetric turbulent wakes with new nonequilibrium similarity scalings. Phys Rev Lett 2013;111:144503.